

## The electric non-dipole effect in strong-field ionization

A. Hartung<sup>1</sup>, S. Brennecke<sup>2</sup>, K. Lin<sup>1,\*</sup>, D. Trabert<sup>1</sup>, K. Fehre<sup>1</sup>, J. Rist<sup>1</sup>, M. S. Schöffler<sup>1</sup>, T. Jahnke<sup>1</sup>, L. Ph. H. Schmidt<sup>1</sup>, M. Kunitski<sup>1</sup>, M. Lein<sup>2</sup>, R. Dörner<sup>1,†</sup> and S. Eckart<sup>1‡</sup>

<sup>1</sup> Institut für Kernphysik, Goethe-Universität, Max-von-Laue-Str. 1, 60438 Frankfurt, Germany

<sup>2</sup> Institut für Theoretische Physik, Leibniz Universität Hannover, Appelstr. 2, 30167 Hannover, Germany

(Dated: April 18, 2022)

Strong-field ionization of atoms by circularly polarized femtosecond laser pulses produces a donut-shaped electron momentum distribution. Within the dipole approximation this distribution is symmetric with respect to the polarization plane. The magnetic component of the light field is known to shift this distribution forward. Here, we show that this *magnetic* non-dipole effect is not the only non-dipole effect in strong-field ionization. We find that an *electric* non-dipole effect arises that is due to the position dependence of the electric field and which can be understood in analogy to the Doppler effect. This *electric* non-dipole effect manifests as an increase of the radius of the donut-shaped photoelectron momentum distribution for forward-directed momenta and as a decrease of this radius for backwards-directed electrons. We present experimental data showing this fingerprint of the *electric* non-dipole effect and compare our findings with a classical model and quantum calculations.

The ionization of an atom by the interaction with an electromagnetic wave is often described by only considering the temporal evolution the electric field vector. This is at the heart of the dipole approximation which neglects the magnetic component and the position-dependence of the light field. It is a surprisingly good approximation over a wide range of wavelengths and intensities from the perturbative single-photon ionization regime of the photoelectric effect over multiphoton ionization to strong-field non-relativistic tunnel ionization. Single-photon ionization is dominated by electric dipole transitions [1, 2]. The same holds in the non-relativistic strong-field regime where it is the time-dependent *electric* field that drives tunnel ionization and determines the electron momentum distribution in a good approximation [3, 4]. Within the dipole approximation, the momentum distribution of the emitted electrons is forward-backward symmetric for single-photon ionization [5] as well as for strong-field ionization [6].

The leading physical mechanisms which eventually lead to a failure of the dipole approximation and a breaking of the forward-backward symmetry of electron emission are different for single-photon and strong-field ionization. For single-photon ionization the dominating term beyond electric dipole transitions is due to electric quadrupole transitions. The interference between electric dipole and electric quadrupole transitions leads to a breaking of the symmetry and at high photon energies to a forward emission of photoelectrons and backward emission of ions [2, 7–10]. The electric quadrupole transitions are due to the spatial dependence of the electric field whereas the transition amplitudes that are driven by the magnetic component of the field are typically much weaker [2]. In contrast, for strong-field ionization the

breakdown of the dipole approximation [4, 11–15] is commonly argued to be due to the magnetic component of the light field that drives the electron forward via the Lorentz force [16] (for the effect of rescattering see Refs. [17–20]). However, the temporospatial dependence of the electric field has not been discussed so far for strong-field ionization at non-relativistic intensities. Up to now, no experimental evidence has been presented which shows an influence of the temporospatial nature of the light field in strong-field ionization that breaks the forward-backward symmetry. It is the purpose of the present paper to provide that missing experimental evidence and show how the temporospatial dependence of the electric field alters electron momentum distributions in strong-field ionization. We show that electric field driven non-dipole effects are as important as those caused by the magnetic field, if a suitable observable is looked at.

We consider circularly polarized light, to avoid the additional complexity caused by recollisions of the electron with its parent ion. Upon ionization of an atom by a circularly polarized, multi-cycle laser pulse at a wavelength of 800 nm the electron momentum distribution has a donut-like shape (blue shape in Fig. 1(a)). The radius of the donut in momentum space is approximately given by

$$\langle p_r \rangle = A_0 = \frac{E}{\omega}, \quad (1)$$

where  $p_r = \sqrt{p_y^2 + p_z^2}$  is the radial momentum component perpendicular to the light propagation direction,  $E$  is the laser's peak electric field,  $\omega$  is the central frequency of the laser pulse and  $A_0$  is the laser's peak vector potential (atomic units are used unless stated otherwise). When calculated within the dipole approximation,

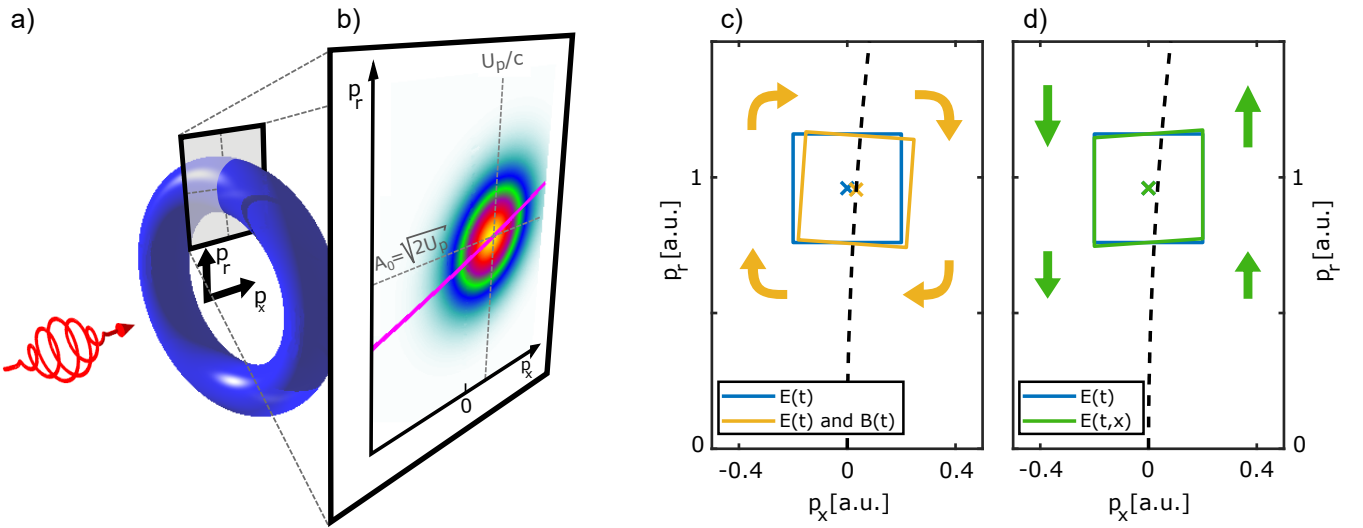


FIG. 1. (a) Illustration of the donut shape of the electron momentum distribution from strong-field ionization in a circularly polarized laser pulse and of the coordinate system that is used throughout our paper. (b) Artist's view of a combination of the two non-dipole effects. The *magnetic* component of the light field drives the donut forward by about  $U_p/c$  through the magnetic part of the Lorentz force. The temporospatial *electric* field results in an increase of  $\langle p_r \rangle$  as a function of  $p_x$  (purple line in (b)). (c) Four classical trajectories are calculated using the dipole approximation. The initial momenta after tunneling are chosen such that the final electron momenta mark the edges of the blue square. Using the same initial conditions but including the magnetic component only (no spatial dependence of the electric field) leads to the yellow quadrangle in (c) which is forward shifted and rotated with respect to the blue square. For the green quadrangle in (d) the temporospatial electric field is considered and the magnetic field is neglected which leads to shearing of the electron momentum distribution as indicated. The crosses indicate the centers of the quadrangles in (c) and (d). For visual representation, both effects are amplified by a factor of 10 (see text).

this donut is symmetric with respect to the polarization plane ( $p_y p_z$ -plane). In pioneering work Smeenk et al. showed experimentally that this momentum distribution is slightly forward shifted by about  $U_p/c$  [11] ( $U_p = \frac{E^2}{2\omega^2}$  is the ponderomotive energy and  $U_p/c$  is the forward momentum which classical mechanics predicts for an electron launched with zero initial velocity and accelerated by a circularly polarized *spatially homogeneous* electromagnetic field.) Soon after, Klaiber et al. [21] predicted an additional forward shift of  $I_p/(3c)$  (with the ionization potential  $I_p$ ) which was confirmed by other calculations [12, 22, 23] and an experiment [24]. In all cases, these forward shifts were discussed to be due to the magnetic component of the light field.

Fig. 1(b) shows an artist's view of the full non-dipole effect in strong-field ionization (including the magnetic and the electric non-dipole effect) in cylindrical coordinates ( $p_x$ ,  $p_r$ ). To further investigate these non-dipole effects, we use classical trajectory simulations (CTS) consisting of two steps. In the first step the electron is freed by laser-induced tunnel ionization. In a second step the electron's acceleration in the time- and position-dependent electromagnetic field is described classically by Newton's equation. For this second step the Coulomb interaction of the electron and its parent ion are not taken into account. The CTS model is well-suited to distinguish electric and magnetic field driven non-dipole effects. We

assume adiabatic tunneling, i.e. that after tunneling the electrons have zero initial velocity in tunnel direction and their velocity in both directions perpendicular to the tunnel direction is described by a rotationally-symmetric initial Gaussian momentum distribution that is centered at zero momentum (analogous to Eq. (9) of Ref. [25]). The electric and magnetic field of the circularly polarized laser pulse are defined by:

$$\vec{E}(x, t) = E_0(t) \begin{pmatrix} 0 \\ \cos(\omega t - \zeta \frac{\omega}{c} x) \\ \sin(\omega t - \zeta \frac{\omega}{c} x) \end{pmatrix},$$

$$\vec{B}(x, t) = \chi \frac{E_0(t)}{c} \begin{pmatrix} 0 \\ -\sin(\omega t - \zeta \frac{\omega}{c} x) \\ \cos(\omega t - \zeta \frac{\omega}{c} x) \end{pmatrix}. \quad (2)$$

Here,  $E_0(t)$  is the temporal envelope of the light pulse. For a real light pulse one sets  $\zeta = \chi = 1$  while in the dipole approximation one sets  $\zeta = \chi = 0$ .

Taking only the magnetic field into account (neglecting the spatial dependence of the electric field,  $\zeta = 0$ ) leads to the well-known forward shift of the donut-shaped electron momentum distribution by  $U_p/c$  [11] and an additional internal rotation of the electron momentum distribution around its center by an angle of about  $A_0/c$  as schematically illustrated in Fig. 1(c). Importantly, the most probable radial momentum  $\langle p_r \rangle$  of the distribution as a function of  $p_x$  remains constant in this case.

scenario	light field's definition	$\zeta$	$\chi$	$\alpha$
T	$\vec{E}(t)$ , no magnetic field	0	0	0.00
U	$\vec{E}(t), \vec{B}(t)$	0	1	0.00
V	$\vec{E}(\vec{x}, t)$ , no magnetic field	1	0	1.07
W	$\vec{E}(\vec{x}, t), \vec{B}(t)$	1	1	1.07

TABLE I. The parameter  $\alpha$  at  $p_x = 0$  a.u. is determined from the CTS model for various scenarios regarding the definition of the electromagnetic field (Eq. (2)) using a  $\sin^2$ -envelope with a total duration of 12 cycles.

In full analogy, the effect of the temporospatial dependence of the electric field  $\vec{E}(x, t)$  alone (neglecting the magnetic field,  $\chi = 0$ ) can be included in the calculations. The temporospatial electric field  $\vec{E}(x, t)$  leads to a shearing of the final momentum distribution as compared to an electric field  $\vec{E}(t)$  that is only time-dependent. The distortion of the electron momentum distribution is schematically illustrated in Fig. 1(d).

Strikingly, the increase of the radius of the donut-shaped electron momentum distribution as a function of  $p_x$ , which is shown in Fig. 1(b) from an artist's perspective, can be interpreted in analogy to the Doppler effect. In the lab frame, electrons that propagate parallel [anti-parallel] to the light-propagation direction experience an oscillating force with a frequency that is lower [higher] than the central frequency of the incident laser field. The frequency of this oscillating force is given by  $\bar{\omega}(p_x) = \omega(1 - p_x/c)$  for a light propagation direction that is parallel to  $p_x$ . Using this insight, e.g. neglecting the Coulomb potential after tunneling and the non-adiabatic offsets of the initial momentum distribution [26] one can approximate the most probable radial electron momentum  $\langle p_r \rangle$  for a given value of  $p_x$ . To this end Eq. 1 is generalized using  $\bar{\omega}(p_x)$  instead of  $\omega$  which leads to

$$\langle p_r \rangle(p_x) = \frac{E}{\bar{\omega}(p_x)} \approx \left(1 + \alpha \frac{p_x}{c}\right) A_0 \quad (3)$$

where  $\alpha = 1$  in this simplest case. Later, we will use  $\alpha$  as a fitting parameter to analyze the *electric* non-dipole effect in experimental data and compare the results to more sophisticated theoretical models. But in a first step, the parameter  $\alpha$  is extracted from our CTS simulations for several scenarios that are summarized in Tab. 1. It is evident that  $\alpha \approx 1$  if the temporospatial dependence of the electric field ( $\vec{E}(x, t)$ ) is taken into account (scenarios V and W in Tab. 1). In particular, the magnetic field does not significantly change the value of  $\alpha$ .

The shearing of the momentum distribution which is induced by the *electric* non-dipole effect and quantified by the value of  $\alpha$  has not yet been described to the best of our knowledge. The key point of the present paper is to show this shearing in an experiment and in numerical *ab-initio* simulations of the TDSE (time-dependent Schrödinger equation). We find significant deviations of  $\langle p_r \rangle(p_x)$  to the expectation from the dipole approxima-

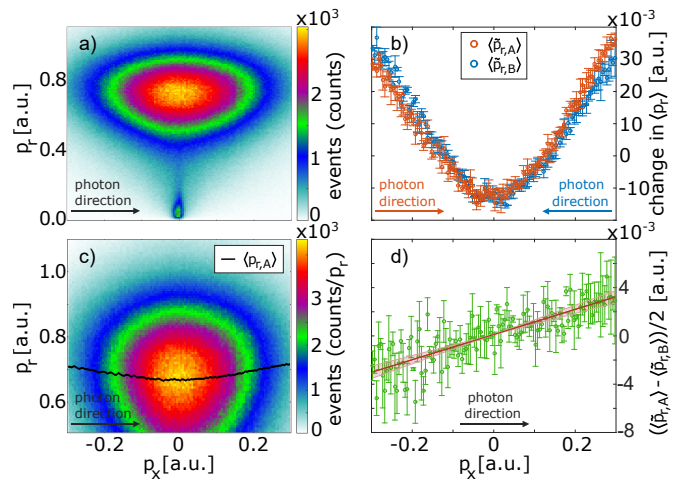


FIG. 2. Experiment on the strong-field ionization of xenon by circularly polarized light at a wavelength of 800 nm and an intensity of  $8.1 \cdot 10^{13} \text{ W/cm}^2$ . (a) shows the electron momentum resolved on the momentum along the light propagation-direction,  $p_x$ , and the radial momentum in the plane of polarization,  $p_r = \sqrt{p_y^2 + p_z^2}$ , for a laser beam that has a propagation-direction as indicated ( $k_{\text{ph}} > 0$ ). (c) shows the same as (a) but zooming in and showing the most probable radial momentum,  $\langle p_r, A \rangle$ , as a function of  $p_x$  (black line). The red data points  $\langle \tilde{p}_r, A \rangle$  in (b) show the same as the black line in (c) after subtracting a constant value (see text). The blue data points,  $\langle \tilde{p}_r, B \rangle$ , show the analogue to the red data points but for an inverted light propagation-direction ( $k_{\text{ph}} < 0$ ). (d)  $S(p_x) = \frac{\langle \tilde{p}_r, A \rangle(p_x) - \langle \tilde{p}_r, B \rangle(p_x)}{2}$  is shown in green. The red line is a linear fit to the green data points using  $\alpha$  as a free parameter for  $S(p_x) = \alpha \frac{p_x}{c} A_0$ . The value of  $\alpha A_0/\text{a.u.} = 1.43 \pm 0.23$  is obtained from the linear fit and is used as a figure of merit to describe the *electric* non-dipole effect. The error bars show the standard deviation of the statistical errors.

tion and will conclude that these deviations are due to the temporospatial dependence of the electric field.

The experiment was performed using the same specialized COLTRIMS reaction microscope [27] and the same laser setup as in Ref. [24]. The 25-fs laser pulses with a central wavelength of 800 nm and a repetition rate of 10 kHz are split into two counter-propagating pathways A and B. In pathway A [B] the light propagation-direction is parallel [anti-parallel] to  $p_x$  and thus the light's wavevector  $k_{\text{ph}}$  is positive [negative]. In both pathways lambda-quarter and lambda-half waveplates ensure that the laser pulses that enter the vacuum chamber are circularly polarized. The two pulses are focused from opposite sides to the same spot in the xenon-gas jet. A static electric field of 27.4 V/cm is used to guide the electrons to a position and time sensitive delay-line detector [28]. The acceptance angle of the electrons in the electron spectrometer is limited. Therefore, only electrons with  $|p_y|/p_r < \sin(8^\circ)$  are considered for the experimental results ( $p_z$ -direction is the time-of-flight direction). Shutters in pathways A and B toggled between

using the two possible pathways. This procedure allows us to eliminate most systematical errors which is essential, since the expected changes of the radius of the donut are on the order of 0.001 a.u. The intensity of the laser pulses in the focus is  $8.1 \cdot 10^{13} \text{ W/cm}^2$  (peak electric field of 0.034 a.u.). The intensity has been calibrated from the most probable radial momentum  $\langle p_r \rangle = 0.68 \text{ a.u.}$  taking non-adiabaticity into account [26].

Figure 2(a) shows the measured electron momentum distribution in cylindrical coordinates after integration over the angle in the polarization plane (see Figs. 1(a) and 1(b)). Fig. 2(c) shows the same data as Fig. 2(a) after restricting the momenta to  $0.5 \text{ a.u.} < p_r < 1.1 \text{ a.u.}$  The forward shift of the electrons with  $0.5 \text{ a.u.} < p_r < 1.1 \text{ a.u.}$  that is due to the magnetic field is not visible in Fig. 2(c) because it is only  $\langle p_x \rangle = 0.0021 \pm 0.0001 \text{ a.u.}$  (value has been determined by a Gaussian fit). This forward shift is due to the magnetic field and can be compared with the theoretically expected value  $\langle p_x \rangle \approx p_r^2/(2c) + I_p/(3c) = 0.0027 \text{ a.u.}$  for  $p_r = 0.68 \text{ a.u.}$  [24]. (The experimental uncertainty of  $\langle p_x \rangle$  only takes the statistical error into account.)

From the data shown in Fig. 2(c), we have determined the most probable radial momentum using a Gaussian fit for every bin along  $p_x$ . The maximum of these Gaussian fits is shown by the black line and referred to as  $\langle p_{r,A} \rangle$ . The values of  $\langle p_{r,A} \rangle$  as a function of  $p_x$  have a close to parabolic shape. In a next step the light propagation-direction is inverted in the experiment and the analysis is done again and the result is referred to as  $\langle p_{r,B} \rangle$ . For each of the two resulting close to parabolic shapes the mean is subtracted using  $\langle \tilde{p}_{r,A} \rangle(p_x) = \langle p_{r,A} \rangle(p_x) - q_A$  and  $\langle \tilde{p}_{r,B} \rangle(p_x) = \langle p_{r,B} \rangle(p_x) - q_B$ . Here, the scalar value  $q_A$  is the mean in  $p_r$  obtained from a Gaussian fit using the projection of the data shown in Fig. 2(c).  $q_B$  is the mean for pathway B in full analogy.

The results for  $\langle \tilde{p}_{r,A} \rangle$  and  $\langle \tilde{p}_{r,B} \rangle$  are presented in Fig. 2(b). Within the dipole approximation the close to parabolic shape would be forward-backward symmetric and the  $p_x$  dependence would be caused by non-adiabatic effects and Coulomb interaction of the electron with its parent ion after tunneling [26]. To disentangle the symmetric contributions from the non-dipole effects, the difference

$$S(p_x) = \frac{\langle \tilde{p}_{r,A} \rangle(p_x) - \langle \tilde{p}_{r,B} \rangle(p_x)}{2} \quad (4)$$

is shown in Fig. 2(d). The slope of  $S(p_x) = \alpha A_0 p_x / c$  is found by fitting and we obtain a value of  $\alpha = 2.38 \pm 0.38$  (which includes the statistical error only). We estimate the systematic error of  $\alpha$  to be  $\pm 0.42$ . As suggested by the illustration in Fig. 1(b), we find that  $\langle p_r \rangle(p_x)$  linearly increases as a function of  $p_x$  for  $k_{\text{ph}} > 0$ . Thus, the electrons flying in the forward direction show a larger radial momentum than those that are emitted into the backward direction. So qualitatively, the experimental

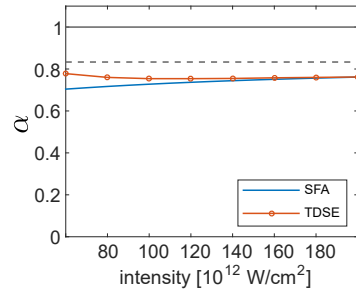


FIG. 3. Dependence of  $\alpha$  at  $p_x = 0 \text{ a.u.}$  on the intensity for a xenon atom at a wavelength of 800 nm that is obtained from a numerical solution of the TDSE (red line) and using the SFA (blue line). The adiabatic limit of  $\alpha = 5/6$  (gray thick dotted line) and the estimate based on Eq. 3 (gray thick solid line) are shown as horizontal lines.

findings are in line with the expectation from Eq. 3.

For a quantitative comparison we have performed numerical simulations of the 3D TDSE including non-dipole effects to first order in  $1/c$  [14, 24] and using an effective potential for xenon [29] converted into a pseudopotential for the 5p state at cutoff radius  $r_{cl} = 2 \text{ a.u.}$  [30]. Based on the corresponding momentum distribution for a short laser pulse with  $\sin^2$ -envelope of 3 cycles total duration, the value of  $\alpha$  is obtained by a fit of the numerically determined dependence of the maximum's position. The obtained values of  $\alpha$  are shown in Fig. 3 for a wide range of intensities. The values of  $\alpha$  are in the range from 0.75 to 0.78 and are systematically smaller than the naively expected value of  $\alpha \approx 1$  (see Tab. 1 and Eq. 3). The quantitative deviations of the experimentally obtained value of  $\alpha$  to the theoretically expected value of  $\alpha$  warrants further research [31].

To deepen our understanding of the electric non-dipole effect theoretically, we have also studied a quantum-orbit model derived from the strong-field approximation [12, 17] (SFA) by application of a saddle-point approximation (analogous to the procedure in Ref. [24]). The resulting values of  $\alpha$  are in good agreement with the TDSE result (see Fig. 3). In particular, this shows that the long-range ionic potential, which is not included in SFA, does not significantly influence the value of  $\alpha$ . The most important difference comparing the SFA to the CTS model is that the SFA incorporates initial momentum offsets, i.e. the initial distribution of the freed electrons is not rotationally-symmetric at the tunnel exit [26]. In leading order of the Keldysh parameter  $\gamma = \sqrt{2I_p}/A_0$  the most probable momentum as a function of  $p_x$  is given by

$$\langle p_r \rangle(p_x) = A_0 + \frac{1}{3A_0} \left( I_p + \frac{p_x'^2}{2} \right) + \frac{A_0}{c} p_x, \quad (5)$$

with the shifted momentum  $p_x' = p_x - (U_p + I_p/3)/c$  (for a light propagation-direction that is parallel to  $p_x$ ). The second quadratic term that is due to non-adiabatic offset momenta is centered around the global maximum

of the momentum distribution. Using Eq. 5 it can be shown, that in the adiabatic limit ( $\gamma \approx 0$ ) the slope of  $\langle p_r \rangle (p_x)$  is characterized by  $\alpha = 5/6$ . However, on the other hand, taking only the magnetic field after tunneling into account ( $\zeta = 0$ ,  $\chi = 1$ ) the model predicts a value of  $\alpha = -1/6$  which can be shown but does not follow directly from Eq. 5.

In conclusion we have found that the temporospatial structure of the electric field ( $\vec{E}(x, t)$ ), that has been so far neglected in the literature on tunnel ionization, alters the momenta of the electrons emitted in strong-field ionization and leads to an *electric* non-dipole effect. Microscopically the *electric* non-dipole effect can be explained by the time-dependent force that acts on the electron in the lab frame. This force is due to the laser field and has a higher frequency for electrons that are traveling anti-parallel to the light propagation-direction than for electrons that travel with the light wave. This change in effective frequency is analogous to the Doppler effect and affects the energy that is transferred to the electron. Thus, the forward-backward symmetry of electron emission in strong-field ionization is broken not only by the well-known *magnetic* non-dipole effect but also by an *electric* non-dipole effect. We expect that the *electric* non-dipole effect will also have an impact on the energetic position of ATI peaks.

## ACKNOWLEDGMENTS

A.H. and K.F. acknowledge support by the German Academic Scholarship Foundation. The experimental work was supported by the DFG (German Research Foundation). K.L. acknowledges support by the Alexander von Humboldt Foundation. S.B., M.L. and S.E. acknowledge funding of the DFG through Priority Programme SPP 1840 QUTIF.

Schmidt, J. B. Williams, R. Dörner, T. Jahnke, M. S. Schöffler, and A. S. Kheifets, “Separating dipole and quadrupole contributions to single-photon double ionization,” *Phys. Rev. Lett.* **121**, 173003 (2018).

- [6] M. Yu. Ivanov, M. Spanner, and O. Smirnova, “Anatomy of strong field ionization,” *J. Mod. Opt.* **52**, 165 (2005).
- [7] A. Sommerfeld and G. Schur, “ber den Photoeffekt in der K-Schale der Atome, insbesondere ber die Voreilung der Photoelektronen,” *Annalen der Physik* **396**, 409 (1930).
- [8] M. J. Seaton, “Momentum transfer in photo-ionization processes,” *Journal of Physics B: Atomic, Molecular and Optical Physics* **28**, 3185 (1995).
- [9] M. Førre and A. S. Simonsen, “Nondipole ionization dynamics in atoms induced by intense xuv laser fields,” *Phys. Rev. A* **90**, 053411 (2014).
- [10] S. Grundmann, M. Kircher, I. Vela-Perez, G. Nalin, D. Trabert, N. Anders, N. Melzer, J. Rist, A. Pier, N. Strenger, J. Siebert, P. V. Demekhin, L. Ph. H. Schmidt, F. Trinter, M. S. Schöffler, T. Jahnke, and R. Dörner, “Observation of photoion backward emission in photoionization of He and N<sub>2</sub>,” *Phys. Rev. Lett.* **124**, 233201 (2020).
- [11] C. T. L. Smeenk, L. Arissian, B. Zhou, A. Mysyrowicz, D. M. Villeneuve, A. Staudte, and P. B. Corkum, “Partitioning of the linear photon momentum in multiphoton ionization,” *Phys. Rev. Lett.* **106**, 193002 (2011).
- [12] P.-L. He, D. Lao, and F. He, “Strong field theories beyond dipole approximations in nonrelativistic regimes,” *Phys. Rev. Lett.* **118**, 163203 (2017).
- [13] S. Chelkowski and A. D. Bandrauk, “Photon-momentum transfer in molecular photoionization,” *Phys. Rev. A* **97**, 053401 (2018).
- [14] S. Brennecke and M. Lein, “High-order above-threshold ionization beyond the electric dipole approximation: Dependence on the atomic and molecular structure,” *Phys. Rev. A* **98**, 063414 (2018).
- [15] N. Haram, R. T. Sang, and I. V. Litvinyuk, “Transverse electron momentum distributions in strong-field ionization: nondipole and coulomb focusing effects,” *Journal of Physics B: Atomic, Molecular and Optical Physics* **53**, 154005 (2020).
- [16] T. Katsouleas and W. B. Mori, “Comment on ‘packet spreading, stabilization, and localization in superstrong fields’,” *Phys. Rev. Lett.* **70**, 1561 (1993).
- [17] M. W. Walser, C. H. Keitel, A. Scrinzi, and T. Brabec, “High harmonic generation beyond the electric dipole approximation,” *Phys. Rev. Lett.* **85**, 5082 (2000).
- [18] M. Dammasch, M. Dörr, U. Eichmann, E. Lenz, and W. Sandner, “Relativistic laser-field-drift suppression of nonsequential multiple ionization,” *Phys. Rev. A* **64**, 061402(R) (2001).
- [19] S. Palaniyappan, A. DiChiara, E. Chowdhury, A. Falkowski, G. Ongadi, E. L. Huskins, and B. C. Walker, “Ultrastrong field ionization of Ne<sup>n+</sup> ( $n \leq 8$ ): Rescattering and the role of the magnetic field,” *Phys. Rev. Lett.* **94**, 243003 (2005).
- [20] A. Emmanouilidou and T. Meltzer, “Recollision as a probe of magnetic-field effects in nonsequential double ionization,” *Phys. Rev. A* **95**, 033405 (2017).
- [21] M. Klaiber, E. Yakaboylu, H. Bauke, K. Z. Hatsagortsyan, and C. H. Keitel, “Under-the-barrier dynamics in laser-induced relativistic tunneling,” *Phys. Rev. Lett.* **110**, 153004 (2013).

\* lin@atom.uni-frankfurt.de

† doerner@atom.uni-frankfurt.de

‡ eckart@atom.uni-frankfurt.de

- [1] M. O. Krause, “Photo-ionization of krypton between 300 and 1500 eV. relative subshell cross sections and angular distributions of photoelectrons,” *Phys. Rev.* **177**, 151 (1969).
- [2] J. W. Cooper, “Photoelectron-angular-distribution parameters for rare-gas subshells,” *Phys. Rev. A* **47**, 1841 (1993).
- [3] L. V. Keldysh, “Ionization in the field of a strong electromagnetic wave,” *Sov. Phys. JETP* **20**, 1307 (1965).
- [4] M. Klaiber, K. Z. Hatsagortsyan, and C. H. Keitel, “Above-threshold ionization beyond the dipole approximation,” *Phys. Rev. A* **71**, 033408 (2005).
- [5] S. Grundmann, F. Trinter, A. W. Bray, S. Eckart, J. Rist, G. Kastirke, D. Metz, S. Klumpp, J. Viehaus, L. Ph. H.

- [22] S. Chelkowski, A. D. Bandrauk, and P. B. Corkum, “Photon momentum sharing between an electron and an ion in photoionization: From one-photon (photoelectric effect) to multiphoton absorption,” *Phys. Rev. Lett.* **113**, 263005 (2014).
- [23] S. Chelkowski, A. D. Bandrauk, and P. B. Corkum, “Photon-momentum transfer in multiphoton ionization and in time-resolved holography with photoelectrons,” *Phys. Rev. A* **92**, 051401(R) (2015).
- [24] A. Hartung, S. Eckart, S. Brennecke, J. Rist, D. Trabert, K. Fehre, M. Richter, H. Sann, S. Zeller, K. Henrichs, G. Kastirke, J. Hoehl, A. Kalinin, M. S. Schöffler, T. Jahnke, L. Ph. H. Schmidt, M. Lein, M. Kunitski, and R. Dörner, “Magnetic fields alter strong-field ionization,” *Nature Physics* **15**, 1222 (2019).
- [25] N. I. Shvetsov-Shilovski, M. Lein, L. B. Madsen, E. Räsänen, C. Lemell, J. Burgdörfer, D. G. Arbó, and K. Tókési, “Semiclassical two-step model for strong-field ionization,” *Phys. Rev. A* **94**, 013415 (2016).
- [26] S. Eckart, K. Fehre, N. Eicke, A. Hartung, J. Rist, D. Trabert, N. Strenger, A. Pier, L. Ph. H. Schmidt, T. Jahnke, M. S. Schöffler, M. Lein, M. Kunitski, and R. Dörner, “Direct experimental access to the nonadiabatic initial momentum offset upon tunnel ionization,” *Phys. Rev. Lett.* **121**, 163202 (2018).
- [27] J. Ullrich, R. Moshammer, A. Dorn, R. Dörner, L. Ph. H. Schmidt, and H. Schmidt-Böcking, “Recoil-ion and electron momentum spectroscopy: reaction-microscopes,” *Rep. Prog. Phys.* **66**, 1463 (2003).
- [28] O. Jagutzki, A. Cerezo, A. Czasch, R. Dörner, M. Hattas, M. Huang, V. Mergel, U. Spillmann, K. Ullmann-Pfleger, T. Weber, H. Schmidt-Böcking, and G. D. W. Smith, “Multiple hit readout of a microchannel plate detector with a three-layer delay-line anode,” *IEEE Trans. Nucl. Sci.* **49**, 2477 (2002).
- [29] X. M. Tong and C. D. Lin, “Empirical formula for static field ionization rates of atoms and molecules by lasers in the barrier-suppression regime,” *Journal of Physics B: Atomic, Molecular and Optical Physics* **38**, 2593 (2005).
- [30] N. Troullier and José Luís Martins, “Efficient pseudopotentials for plane-wave calculations,” *Phys. Rev. B* **43**, 1993 (1991).
- [31] Analysis of another data set for the strong field ionization of argon using circularly polarized light at 800 nm yields a value of  $\alpha = (1.315 \pm 0.485)/(A_0/\text{a.u.}) = 1.69 \pm 0.62$  using  $A_0 = 0.78 \text{ a.u.}$  (see Fig. 6.57 in Ref. [32]).
- [32] A. Hartung, “Der Photonenimpuls in der Starkfeldionisation,” Ph.D. thesis, Goethe University Frankfurt, Frankfurt am Main (Germany) (2019).